Metal Film over Nanosphere (MFON) Electrodes for Surface-Enhanced Raman Spectroscopy (SERS): Improvements in Surface Nanostructure Stability and Suppression of Irreversible Loss

Lisa A. Dick,† Adam D. McFarland, Christy L. Haynes, and Richard P. Van Duyne*

Department of Chemistry, Northwestern University, Evanston, Illinois 60208-3113

Received: September 27, 2001; In Final Form: November 23, 2001

The stability and reproducibility of most SERS-active electrode surfaces are far from ideal. We have focused on this problem by developing and characterizing a metal film over nanosphere (MFON) electrode which solves these shortcomings. Atomic force microscopy (AFM), cyclic voltammetry, and surface-enhanced Raman spectroscopy (SERS) of representative molecules were used to characterize and evaluate the electrochemical and SERS performance of MFON electrodes. Tremendous stability to extremely negative potential excursions is observed for MFON electrodes as compared to standard metal oxidation reduction cycle (MORC) roughened electrodes. Consequently, irreversible loss of SERS intensity at negative potentials is not observed on these MFON electrodes. We conclude that MFON electrodes present a significant advantage over MORC electrodes because SERS enhancement is not lost upon excursion to extremely negative potentials. This work demonstrates that the MFON substrate, while easily prepared and temporally stable, offers unprecedented stability and reproducibility for electrochemical SERS experiments. Furthermore, one can conclude that irreversible loss is not a distinguishing characteristic of electrochemical SERS and consequently cannot be used as evidence to support the chemical enhancement mechanism.

I. Introduction

Surface-enhanced Raman scattering (SERS) is widely used to acquire vibrational spectra from adsorbates on roughened metal surfaces. To date, many review articles[1−4] have been published on SERS affording a comprehensive overview of the field. Furthermore, several application-specific reviews of SERS have been written for chemical detection,[5] electrochemistry,[6] medicine,[7,8] biochemistry,[9] and UHV surface science.[10]

SERS possesses many desirable characteristics as a tool for the chemical analysis of interfacial molecular species including high specificity, attomole to high zeptomole mass sensitivity, micromolar to picomolar concentration sensitivity, and interfacial generality.[11,12] However, SERS also has some characteristic weaknesses[12] that have limited its use in analytical applications, such as (1) molecularly selective detectors for flow injection analysis, high performance liquid chromatography, and capillary zone electrophoresis; (2) chemical sensors for environmental and process monitoring; and (3) biosensors for clinical use. The most problematic weakness, in this context, is the extreme sensitivity of the surface enhancement factor (EF) to the nanostructure of the active surface. This, coupled with the difficulties associated with reproducibly fabricating the nanostructure of many common SERS-active surfaces (viz., metal oxidation−reduction cycle (MORC) roughened electrodes, colloids, and vapor-deposited metal island films), leads to less than ideal sample consistency. Although the metastable nature of the common SERS-active surfaces with respect to thermal, potential-dependent, and concentration-dependent perturbations hinders some applications, many important experiments are still possible. One example is the combined use of thermal desorption spectroscopy with SERS in ultrahigh vacuum (UHV) experiments to measure site-specific adsorbate binding energies and vibrational spectra.[13] Other examples include concentration-jump or potential step studies of adsorption/desorption kinetics at electrode or colloid surfaces,[14] and the use of ultrafast, pulsed laser excitation to probe vibrational relaxation, energy transfer, or electron dynamics at surfaces.[15,16]

In addition to the practical matters of reproducibility, stability, and utility of SERS-active surfaces in various experimental situations, the acceptance of SERS as a general research tool has been hindered by continuing uncertainties with regard to the fundamental mechanism(s) of the surface-enhancement phenomenon itself. The SERS community agrees that two simultaneously operative enhancement mechanisms, each with its own characteristic size-scale of surface roughness, are responsible for the total surface enhancement factor (EF) of 10^6 in conventional SERS. Large scale roughness in the 10−100 nm range is believed to contribute a factor of 10^4 to the overall EF through a long-range, classical, electromagnetic (EM) enhancement mechanism.[17−19] The EM mechanism is based on the amplified electromagnetic fields generated upon excitation of the localized surface plasmon resonance (LSPR) of nanoscale surface roughness features.[20] Atomic scale roughness,[21,22] visualized as individual adatoms or small adatom clusters, is thought to be the crucial structural feature of the short-range chemical (CHEM) enhancement mechanism which contributes an additional EF $= 10^1-10^2$. Furthermore, the CHEM mechanism is regarded as a type of metal electron-mediated resonance Raman spectroscopy (RRS) that involves increased electron-photon coupling and transient charge transfer into the affinity levels of the adsorbate.[23,24,2] Recent observation of single molecule SERS signals, with total enhancement factors of 10^{14}, has both renewed the interest in the investigation of SERS

* To whom correspondence should be addressed. E-mail: vanduyne@chem.northwestern.edu.

† 3M Corporation, St. Paul, MN.

10.1021/jp013638l CCC: $22.00
Published on Web 12/27/2001

enhancement mechanisms and challenged the understanding of the partitioning of the total enhancement into EM and CHEM contributions. Current experimental evidence suggests that the EM enhancement mechanism plays a large role in single molecule SERS but falls some 4−6 orders of magnitude short of accounting for an enhancement factor of 10^{14}.[25−27]

The EM mechanism has several experimental signatures: (1) surface-enhanced Raman excitation spectra (SERES) that depend sensitively on surface nanostructure, the optical dielectric response functions of the metal, and the dielectric constant of the medium surrounding the roughened metal surface;[28−30] (2) the long-range (viz., a few nanometers) distance dependence;[31−33] (3) weak dependence of the EF on the chemical identity of the adsorbate;[3] and (4) the existence of surface-enhanced second harmonic generation (SESHG),[34−36] surface-enhanced hyper-Raman scattering(SEHRS),[37,38] and other surface-enhanced spectroscopies (SES). In comparison, the involvement of the CHEM mechanism is manifested in a more subtle manner through (1) irreversible loss phenomena both in electrochemical-SERS (ECHEM-SERS)[39,40] and UHV-SERS;[10] (2) laser excitation wavelength dependence in plots of SERS intensity vs electrode potential in ECHEM-SERS;[2,41] (3) observation of "first layer" SERS;[42,43] (4) strong dependence of the EF on the chemical identity of the adsorbate;[44] (5) quenching of signals from "active sites" in UHV−SERS by submonolayer coverages of O_2[45] or Pd[46] and in ECHEM-SERS by underpotential deposition (UPD) of submonolayer coverages of Tl,[47] Cd,[48] and Pb[49,50] on AgORC electrodes; and 6) thermal quenching of SERS of pyridine and H_2O at AgORC electrodes.[51,52]

In this paper we report, in detail, on the fabrication and characterization of a new electrode for ECHEM-SERS that does not require any pretreatment step, as does the MORC, to render it SERS-active. This electrode is a variant of the metal film over nanosphere (MFON) SERS-active surface previously studied in air[11,53] and UHV.[13] Although vapor deposition of metal films over supported particles has previously been used to generate SERS-active substrates for analytical studies,[13,54−57] it has not been used to fabricate SERS-active electrodes or to advance the mechanistic understanding of SERS.

Atomic force microscopy (AFM) is used to examine the nanostructure of AgFON electrodes, and cyclic voltammetry of the reversible redox couple $Ru(NH_3)_3^{3+}/Ru(NH_3)_3^{2+}$ is used to evaluate the electrochemical performance of AgFON and AuFON electrodes. The vibrational spectroscopy of the $Ru(NH_3)_3^{3+}/Ru(NH_3)_3^{2+}$ redox couple, *trans*-1,2-bis(4-pyridyl)-ethylene (BPE), and pyridine are studied on AgFON electrodes by ECHEM-SERS. Each of these adsorbates represents a different class of adsorption behavior. The $Ru(NH_3)_3^{3+}/Ru(NH_3)_3^{2+}$ system was chosen as an example of weak reversible adsorption, BPE was chosen because it exhibits strong irreversible adsorption, and pyridine, the universal model system for SERS studies, exemplifies a system that is reversibly adsorbed with intermediate strength.

The MFON fabrication technique reported here represents an enormous improvement over MORC electrodes. Surface roughness produced by vapor deposition of a SERS-active metal over a nanosphere monolayer is extremely reproducible, as well as temporally stable on the time scale of many days (when protected from atmospheric surface contamination). In addition, it is vastly more stable to thermal, concentration, and electrochemical potential perturbations. New SERS experiments can also be carried out with MFON electrodes that were previously not possible with either in situ or ex situ MORC electrodes. For example, one can now vary the concentration or chemical nature of the supporting electrolyte in order to study its effect on a surface electrode reaction without simultaneously changing the nature of the surface roughness and, therefore, the surface EF. We have exploited this feature of MFON electrodes in studies of adsorbate surface symmetry as detected by SEHRS[38,58] and in SERS experiments designed to probe the electrostatic binding of cytochrome *c* to *ω*-mercaptocarboxylic acid self-assembled monolayers formed on MFON substrates.[55]

This work further demonstrates that the irreversible loss phenomenon is strongly suppressed with MFON as compared to MORC electrodes. Accordingly, the following new questions about the SERS enhancement mechanism can be posed: (1) is irreversible loss actually just reflection of the metastable nature of atomic scale roughness and, therefore, a valid signature of the CHEM enhancement mechanism? or (2) is irreversible loss actually associated with the morphological instability of nanometer scale roughness and consequently a signature of the EM mechanism?

The most frequent explanation given for the existence of the irreversible loss phenomena in SERS has been based on the presumed presence of adatoms or adatom clusters and their role in the CHEM enhancement mechanism. During an ORC, both large scale and small scale (adatoms) roughness features are generated. Adatoms, which would energetically prefer to migrate from a terrace site to a kink site and finally to a bulk lattice site, are instead stabilized by association with halides, other adsorbates, or even water. Upon excursion to sufficiently negative potentials, halides and/or other adsorbates are desorbed, allowing adatoms to migrate to and ultimately occupy bulk Ag lattice sites. As a result, when the potential is returned to the point that halides and other molecules readsorb, SERS activity is not restored. Similarly, as the temperature of a system is raised, adatom mobility increases and they are allowed to migrate to the bulk Ag lattice. In the case of UPD with metal adlayers, atomic scale roughness features destroyed during deposition are not reformed upon stripping of the metal adlayer.

As a result of these presumptions, several studies have been carried out to determine the morphological properties of Ag films which undergo irreversible loss. In situ electrochemical scanning tunneling microscopy studies have shown both large and atomic scale changes on roughened Ag surfaces upon shifting the applied potential toward negative values.[39,59] Ex situ scanning electron microscopy experiments by Pemberton and co-workers[60,61] revealed that the strongest signals for pyridine were obtained on AgORC electrodes with nodule diameters near 120 nm. However, upon cathodic quenching which presumably destroyed adatoms, but not large scale roughness features, 75% of the SERS signal was lost. The hypothesis advanced was that changes on the smaller, adatom scale were responsible for the observed signal changes. Otto and co-workers attribute signal loss and partial recovery to regeneration of SERS-active sites or trapping of pyridine and Cl^- in grain boundaries.[40]

An interesting contrast to these studies is afforded by those of Weaver and co-workers in which SER spectra for benzene, acetylene and related molecules adsorbed on AuORC electrodes modified with 1−3 monolayer thick films of Rh,[62,63] Ru,[62,63] and Pt[63] are still observed.

The remainder of this paper is organized as follows. In section II, the techniques used for fabrication and characterization of MORC and MFON SERS-active electrodes are described. In section III, the electrochemistry of smooth metal electrodes, MORC electrodes, and MFON electrodes are compared. This section also includes SERS data captured from ruthenium hexaammine, BPE, and pyridine on AgFON electrodes. In the

case of pyridine on a AgFON electrode, the absence of irreversible loss is demonstrated. Section IV summarizes our results and conclusions.

II. Experimental Section

A. Chemicals. $NaClO_4$ was purchased from G. Frederick Smith Chemical Co. (Powell, OH), KCl from Mallinckrodt, Inc. (Phillipsburg, NJ), pyridine from Fisher Scientific (Fairlawn, VA), ruthenium hexaammine trichloride from Strem Chemicals, Inc. (Newburyport, MA), and prepurified nitrogen from Union Carbide Corp., Linde Division (Wilmington, CA). Water was obtained from a Milli-Q (Millipore, Inc., Marlborough, MA) purification system. The BPE was purchased from Aldrich (Milwaukee, WI) and purified by sublimation.

B. Atomic Force Microscopy. Images were recorded using a Nanoscope II microscope (Digital Instruments, Inc., Santa Barbara, CA) and Si_3N_4 cantilevers (force constant 0.15 N/m). The images reported herein are raw, unfiltered data collected in constant force mode using a scan rate of 8 lines/s. The range of the scan head was 1.2 μm × 1.2 μm.

C. Electrochemistry. Studies were conducted on smooth Ag and Au working electrodes embedded into a single glass body. Thus, comparisons between behavior on different surfaces could be made under identical conditions. Metal wires were obtained from D. F. Goldsmith (Evanston, IL) and flamed into balls to make larger area electrodes (0.02−0.04 cm^2). Short segments of the flamed wires were then mechanically connected to longer insulated copper leads. The electrodes were embedded into a glass capillary tube using Torr Seal (Varian Vacuum Products, Lexington, MA). Before use, surfaces were polished with 5.0, 1.0, 0.1, and 0.05 μm alumina (Buehler Ltd., Lake Bluff, Illinois) and rinsed with high purity water and methanol.

The electrochemical cell has been previously described.[64] The reference electrode was a saturated Ag/AgCl with a Pt leak, the auxiliary electrode was Pt wire, and the working electrode was Ag or Au. The potentiostat and cyclic voltammetry data acquisition program were locally developed.

The Raman spectroelectrochemical cell[14,65] was also a three electrode design with the same components as listed for the electrochemical cell. It was designed so that a laser beam would be able to enter and exit the cell after reflecting off of the electrode surface while traversing a minimal solution volume.

Digital simulations of cyclic voltammetric responses for ruthenium hexaammine were conducted with the use of the program CVSIM on the basis of the explicit finite difference algorithm.[66] The parameters used were $D = 6.2 \times 10^{-6}$ cm^2 s^{-1},[67] $\alpha = 0.65$, and k_{sh}=0.35 cm s^{-1}. [68]

D. Raman Spectroscopy. A Spectra Physics model 124B HeNe laser was used for the excitation wavelength of 632.8 nm. A Spectra Physics model 3900 Ti:Al_2O_3 laser pumped by a Spectra Physics model 171−18 Ar^+ laser was used for the excitation wavelength of 752.0 nm. Raman scattered radiation was detected using either a SPEX Model 1401-II double-grating monochromator equipped with a water-cooled RCA C31034A-02 PMT or an ACTON VM-505 single grating monochromator equipped with a Photometrics PM-512 CCD detector. In the latter system, holographic edge filters (Physical Optics Corp., Torrance, CA, and Kaiser Optical Systems, Ann Arbor, MI) were used to reject the excitation and Rayleigh scattered light.

E. AgORC Surface Preparation. Oxidation−reduction procedures were utilized for ex situ and in situ electrochemical roughening of Ag electrodes. For in situ roughening, a double potential step between −0.2 V and +0.2 V (vs Ag/AgCl) was performed such that 25 mC/cm^2 of charge was passed in the presence of 0.1 M KCl/50 mM pyridine. For ex situ roughened surfaces, the ORC was performed in the presence of 0.1 M KCl. While maintaining potential control, 0.1 M KCl/50 mM pyridine was then introduced into the cell. All solutions were deoxygenated by bubbling with N_2 prior to use. During all measurements, N_2 flowed over the solution to maintain an oxygen free environment.

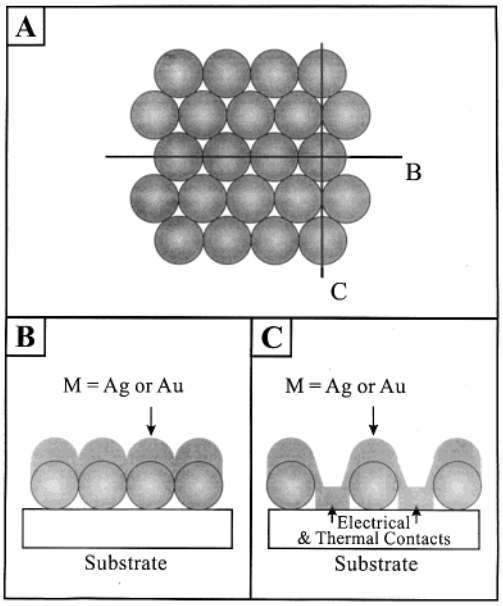

Figure 1. Illustration of electrical and thermal contacts for metal film over nanosphere (MFON) surfaces. (A) Close-packed array of nanospheres, (B) view along a row of nanospheres, and (C) view along a column of nanospheres.

F. MFON Surface Preparation. MFON surfaces were fabricated with the use of a modified Consolidated Vacuum Corporation vapor deposition chamber. The steps included (1) coating a smooth electrode surface with 542 nm diameter surfactant free, white carboxyl polystyrene latex nanospheres (Interfacial Dynamics Corporation, Portland, OR); (2) masking off the area where metal was not desired, (3) depositing a known thickness of metal, and (4) removing the mask. Nanospheres were diluted by a factor of 2 in a 1:800 dilution of TritonX-100 in methanol. During the deposition, pressures in the chamber were $<10^{-6}$ Torr. The deposition source was a tungsten boat (R. D. Mathis, Long Beach, CA) filled with the desired metal. The mass thickness of films was measured with a quartz crystal microbalance which was calibrated by stripping voltammetry[69,70] and AFM of partially masked samples, scanning over the boundary to obtain an average thickness measurement of the deposited film.

III. Results and Discussion

The MFON surfaces central to this study are schematically depicted in Figure 1. In the top portion of Figure 1A, a monolayer of close-packed nanospheres is shown. Following along line B, it can be seen that the metal overlayer does not contact the substrate in this perfect packing arrangement (Figure 1B). However, along line C the metal overlayer contacts the substrate, providing thermal and electrical contacts to the substrate material (Figure 1C). Physical characteristics and the chemical behavior of these MFON surfaces are later discussed based on AFM, cyclic voltammetric, and SERS results.

A. Atomic Force Microscopy. Figure 2 shows an AFM image of a AgFON electrode with Ag mass thickness of 200 nm and nanosphere diameter of 542 nm. In the low-resolution

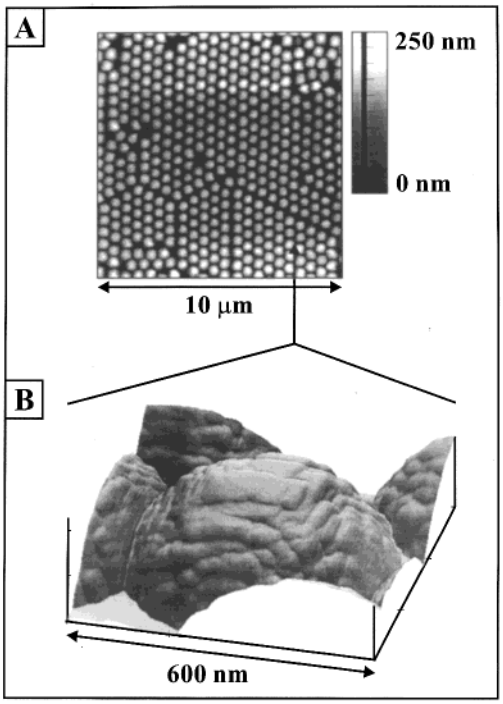

Figure 2. Ambient contact mode atomic force microscope image of 200 nm Ag over 542 nm diameter polystyrene spheres. (A) Array of spheres (10 μm × 10 μm) and (B) image (600 nm × 600 nm) of one sphere showing substructure roughness.

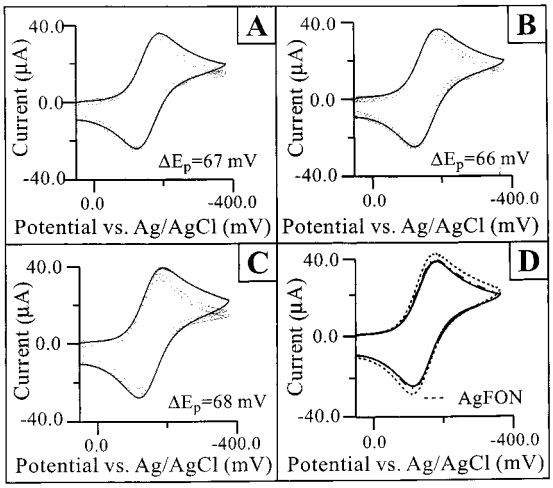

Figure 3. Ag electrode cyclic voltammograms of 5 mM $Ru(NH_3)_6^{3+/2+}$ in 0.5 M KCl. All scans are 100 mV/s. (A) smooth Ag electrode, (B) electrochemically roughened (25 mC/cm^2) Ag electrode, (C) AgFON electrode, and (D) overlay of (A), (B), and (C). Circles are the digital simulation for a smooth Ag electrode.

image (Figure 2A), areas of well packed domains are obvious, as are grain boundaries and vacancies which provide additional electrical and thermal contacts between the metal overlayer and the underlying "smooth" surface. In Figure 2B, the high-resolution image shows that the top of each Ag-coated nanosphere is not smooth but exhibits substructure roughness features of 30−50 nm in size.

B. Electrochemistry. Figures 3 and 4 show the electrochemical behavior of ruthenium hexaammine on three different Ag and two different Au surface preparations. In each of the plots, solid lines are experimental data and circles are theoretical ideal behavior obtained by digital simulation. First, smooth Ag (Figure 3A) shows close to ideal reversible electrochemical behavior with a peak separation of 67(±1) mV. As the cathodic limit is

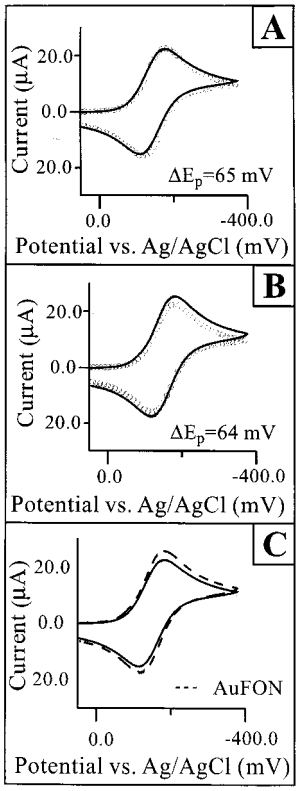

Figure 4. Au electrode cyclic voltammograms of 5 mM $Ru(NH_3)_6^{3+/2+}$ in 0.5 M KCl. All scans are 100 mV/s. (A) smooth Au electrode, (B) AuFON electrode, and (C) overlay of (A) and (B). Circles are the digital simulation for a smooth Au electrode.

approached, there is a slight discrepancy between an ideal electrode and the smooth Ag electrode. This shape discrepancy is also observed in the cyclic voltammogram obtained by Bilewicz and Majda[71] The theoretical model does not account for deviations from ideal reversible behavior such as adsorption of the electroactive species to the surface. Because the discrepancy between the model and experimental results increases at lower electroactive species concentrations, a logical conclusion is that some irreversible adsorption to the surface occurs. Confirmation of this phenomenon is offered in the next section. In Figure 3B, a MORC electrode was tested, showing a peak separation of 66(±1) mV, similar to that obtained on smooth Ag. Behavior of the AgFON electrode is shown in Figure 3C, showing a separation of 68(±1) mV. Additionally, the peak current for the AgFON electrode is higher due to an increase in surface area of the electrode inherent in the preparation procedure. All three curves are overlaid in Figure 3D, showing that any deviation from ideal behavior is intrinsic to the system and is not dependent upon electrode preparation methodology.

Figure 4 addresses the electrochemical behavior on Au surfaces. Figure 4A shows the cyclic voltammogram of ruthenium hexaammine on smooth Au, yielding a peak separation of 65(±1) mV. Similarly, the AuFON prepared electrode shows a separation of 64(±1) mV and nearly ideal shape for reversible electrochemistry (Figure 4B). Figure 4C shows the overlay cyclic voltammograms obtained from smooth Au and AuFON electrodes. Like Ag surfaces, both Au electrode preparations are similarly behaved. Thus, electrochemical characterization shows that MFON electrodes are electrochemically identical to smooth metal and MORC electrodes with respect to reversible electron transfer of ruthenium hexaammine.

For planar electrodes, peak current is proportional to the square root of the scan rate. In Figure 5, the peak current vs

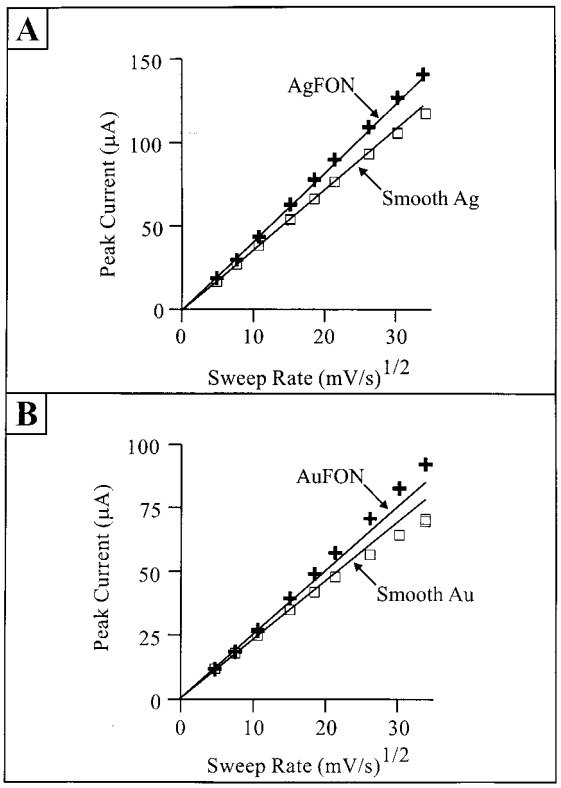

Figure 5. Cyclic voltammetry peak current vs scan rate$^{1/2}$ of 5 mM $Ru(NH_3)_6^{3+/2+}$ in 0.5 M KCl. Solid lines are theory, squares are experimental points for smooth metal, and pluses are experimental points for MFON. (A) M = Ag and (B) M = Au.

square root of scan rate is plotted for MFON and smooth Ag (Figure 5A) and Au (Figure 5B) electrodes. The smooth Ag and Au electrodes show a deviation at high scan rates from theoretical expectations which is likely due to uncompensated resistance. MFON electrodes show ideal behavior up to a scan rate of 250 mV/sec. The cause of the deviation above the theoretical prediction for the AuFON at high sweep rates is currently unknown. The larger slopes for the MFON electrodes in comparison to the MORC electrodes can be attributed solely to the increased microscopic surface area of the MFON electrode as compared to the smooth, polished electrode.

C. Surface-Enhanced Raman Spectroscopy. With the electrochemical performance of MFON electrodes evaluated, the next goal is to test their SERS-activity with several adsorbates that exhibit different electrode binding affinities and kinetics. As an extension of the presented electrochemical work, the spectra of the oxidized and reduced forms of ruthenium hexaammine were obtained (Figure 6). Positively charged ruthenium hexaammine is weakly adsorbed at the positively charged surface. Figures 6A and 6B show the normal Raman scattering and SER spectra of Ru^{3+} species in the solid and solution states. The Ru^{3+}-N stretch is near 500 cm^{-1}.[72] Figure 6C shows that upon excursion of the potential to −0.4 V, the Ru^{2+}-N peak is observed at 460 cm^{-1}.[72]

The spectra of the irreversibly adsorbed molecule BPE (Figure 7) and the reversibly adsorbed molecule pyridine (Figure 8) on several different electrode preparations were obtained for comparison. The in situ and ex situ roughened Ag electrodes produce spectra which are very similar to the AgFON electrode for both BPE and pyridine. Signal intensity is greatest for in situ MORC electrodes. The ex situ MORC and MFON electrode preparations typically yielded signals of comparable intensity which were 60% of the maximum in situ signal. It is significant

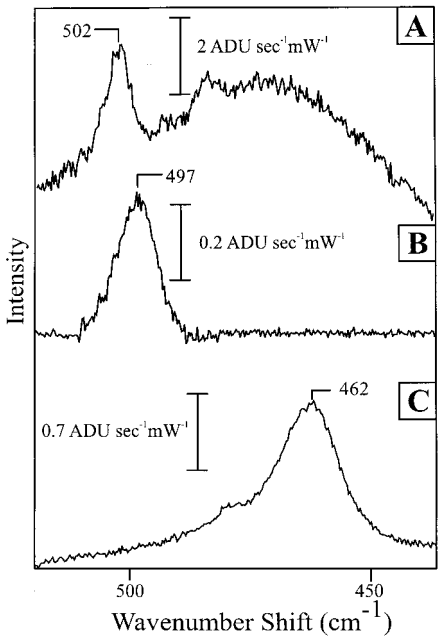

Figure 6. Raman and SER spectra on AgFON of $Ru(NH_3)_6Cl_3$. (A) Normal Raman of solid $Ru(NH_3)_6Cl_3$, (B) SERS of 0.5 mM $Ru(NH_3)_6^{3+}$ in 0.1 M KCl, 0.0 V vs Ag/AgCl, and (C) SERS of 0.5 mM $Ru(NH_3)_6^{2+}$ in 0.1 M KCl, −0.4 V vs Ag/AgCl. Laser excitation was 20 mW 752 nm.

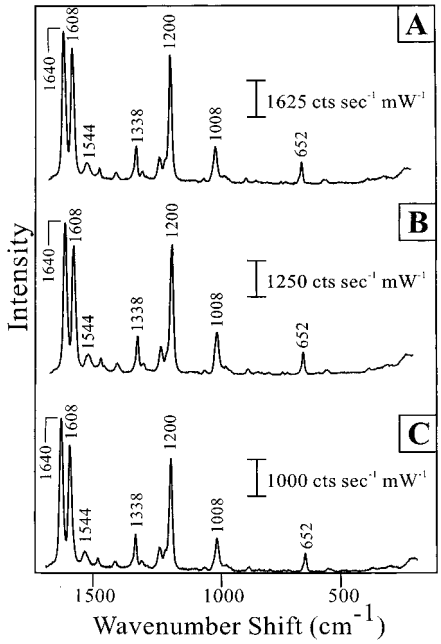

Figure 7. SER spectra of 0.4 mM BPE in 0.1 M KCl at −0.6 V vs Ag/AgCl. (A) In situ AgORC electrode (25 mC/cm^2), (B) ex situ AgORC electrode (25 mC/cm^2), and (C) AgFON electrode. Laser excitation was 4 mW 632.8 nm, scan rate 1 Å/s, 1 s dwell time.

to note that it was not possible to reproduce the spectra with extra lines observed by Garrell and co-workers[73] with the in situ technique, even with widely varying roughening procedures.

With the enhancing ability of the surfaces proven, the studies were extended over a wide potential range. Spectra of pyridine on AgFON surfaces were taken from −0.3 to −1.3 V (Figure 9), showing that the pyridine signal remains even as H_2 evolution is observed. *This demonstrates that SERS can be observed at extremely negative applied potentials.* The signal intensity reaches a maximum at −0.7 V with an excitation wavelength of 632.8 nm. This result is consistent with studies conducted

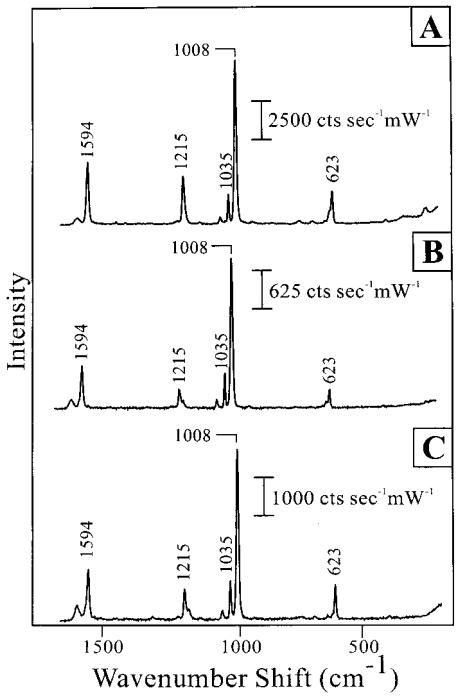

Figure 8. SER spectra of 50 mM pyridine in 0.1 M KCl at −0.7 V vs Ag/AgCl. (A) In situ AgORC electrode (25 mC/cm^2), (B) ex situ AgORC electrode (25 mC/cm^2), and (C) AgFON electrode. Laser excitation was 4 mW 632.8 nm, scan rate 1 Å/s, 1 s dwell time.

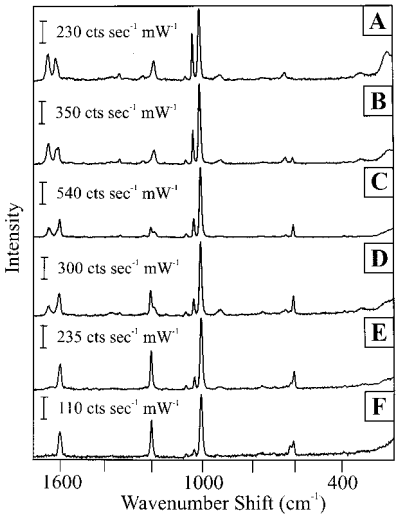

Figure 9. Potential dependence of SER spectra of 50 mM pyridine in 0.1 M KCl on AgFON. (A) −0.3 V, (B) −0.5 V, (C) −0.7 V, (D) −0.9 V, (E) −1.1 V, and (F) −1.3 V vs Ag/AgCl. Laser excitation was 4 mW 632.8 nm, scan rate 1 Å/s, 1 s dwell time.

on other surface preparations but under otherwise similar experimental conditions.[14,74,75]

SERS detected cyclic voltammograms of the 1008 cm^{-1} band (ring breathing mode) of pyridine were performed on AgORC and AgFON electrodes and are shown in Figure 10. Clearly, the AgFON surface (Figure 10A) is far more stable to negative potential excursions than is the AgORC surface. (Figure 10C). Parts B and D of Figure 10 both show the onset of H_2 evolution, between −1.1 and −1.2 V, as the SERS signal is monitored.

Potential stability of the SERS signal of the 1008 cm^{-1} band of pyridine was further studied as the potential was repeatedly stepped and held for 20 s between −0.7 and −1.0 V (Figure 11). An overall signal loss of 80%, with a 50% decrease occurring immediately, was observed for the AgORC electrode

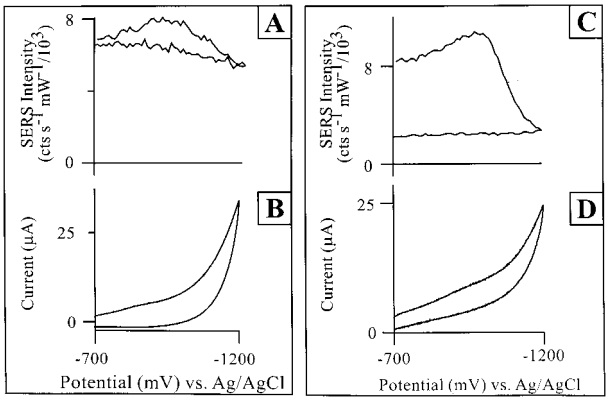

Figure 10. SERS detected cyclic voltammograms. SERS intensity of the 1008 cm^{-1} band of pyridine vs potential. (A) AgFON electrode and (C) in situ AgORC electrode (25 mC/cm^2). Laser excitation was 4 mW 632.8 nm, 0.1 s dwell time, 50 mM pyridine in 0.1 mM KCl. The onset of H_2 evolution from (B) AgFON and (D) AgORC electrodes is indicated by the increase in current between −1.1 and −1.2 V.

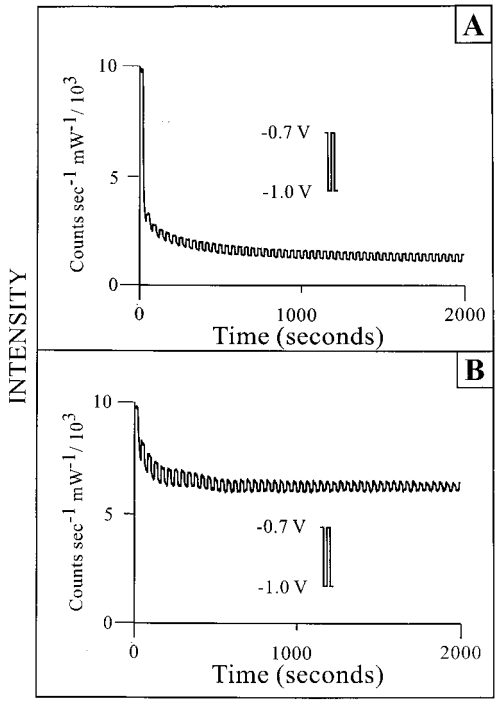

Figure 11. Potential step stability of SERS signal of 50 mM pyridine in 0.1 M KCl obtained from (A) AgORC electrode and (B) AgFON electrode. Laser excitation was 4 mW 632.8 nm.

upon potential cycling. In contrast, the AgFON prepared electrode showed only a 30% reduction in signal followed by a region of complete stability after undergoing the same cycling procedure, and no drastic immediate signal loss was observed. The AFM image (not shown) after cycling reveals a decrease in roughness from 30 to 50 nm to approximately 20 nm. While the 30% reduction in signal intensity can be attributed to this nanoscale restructuring, it is important to recognize that the irreversible loss phenomenon is not observed. The fact that both SERS-activity and nanometer-scale roughness are preserved on AgFON electrodes suggests that nanometer-scale rearrangement may be responsible for the irreversible loss phenomenon observed with MORC electrodes.

Finally, the response of AgORC and AgFON to concentration jump perturbations is shown in Figure 12. Pyridine is flow-injected into the spectroelectrochemical cell containing a AgFON or a AgORC roughened surface under several electro-

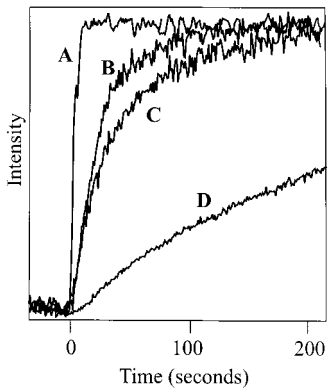

Figure 12. SERS signal growth upon flow injection of as 50 mM pyridine to surface. (A) Instrument response test: 983 cm^{-1} band of 0.5 M Na_2SO_4 introduced to sample cell containing water. (B) AgFON electrode, 0.1 M $NaClO_4$, −0.9 V; (C) AgFON electrode, 0.1 M KCl, −0.7 V; and (D) AgORC electrode, 0.1 M KCl, −0.7 V. Laser excitation was 4 mW 632.8 nm.

lytic conditions. For the AgFON electrode in the presence of ClO_4^- electrolyte, which does not adsorb to the surface, the SERS signal grows in very quickly upon introduction of 50 mM pyridine (Figure 12B). With KCl as electrolyte, the signal at the AgFON surface increases at a slightly slower rate (Figure 12C). In addition, for pyridine introduced to the AgORC electrode in the presence of KCl, it takes 10 times longer for the signal to approach a plateau value (Figure 12D). In each case, the SERS signal rise times are longer than the inherent instrumental response time (Figure 12A). This may be attributed to adsorption kinetics and/or structural rearrangements that are a function of interactions between pyridine, the electrolyte, and the specific nature of the Ag surface. A previous study has suggested that cooperative coadsorption between Cl^- and pyridine is expected according to a Lewis acid model of adsorption.[14] Because AgORC surfaces are more heterogeneous than AgFON surfaces, it is possible that a longer time is necessary for the adsorption of many molecules to occur.

SERS spectra on AuFONs have been obtained using methods analogous to those presented in this work. These spectra have not been included because the studies performed on AuFON substrates are not as thorough as those performed on AgFON substrates, and accordingly, that data will be the subject of a future publication. We regard the data presented herein using AgFONs as the most definitive proof that MFON electrodes are exceptionally stable, reproducible SERS electrodes.

IV. Conclusions

The MFON electrode surface has been shown to exhibit cyclic voltammetric behavior that is consistent with both smooth and electrochemically roughened surfaces. The MFON electrode has been demonstrated to be SERS-active for several representative probe molecules with different adsorption affinities and kinetics. In particular, these surfaces are useful for SERS studies under electrochemical conditions because they do not depend on adsorbed counterions during surface generation. Furthermore, MFON surfaces extend the potential window over which measurements can be made on Ag surfaces and make possible the reproducible generation of SERS-active Ag surfaces which has previously proven difficult. Because SERS enhancement on MFON electrodes is not lost upon excursion to extremely negative potentials, they present a significant advantage over MORC electrodes. This work demonstrates that the MFON substrate, while easily prepared and temporally stable, offers unprecedented stability and reproducibility for electrochemical SERS experiments.

The potential step and SERS-detected cyclic voltammograms show a difference in the amount of signal loss between AgFON and AgORC surfaces, indicating that the irreversible loss phenomenon is not germane to SERS-active surfaces under electrochemical conditions. While irreversible loss *may* occur, it is not a uniquely distinguishing characteristic of *every* SERS-active surface. We contend that because atomic scale roughness behavior is similar on both MFON and MORC electrode surfaces, only changes in nanometer scale roughness induced by negative potential excursions contribute to the differences observed in the SERS intensities. Finally, we conclude that irreversible loss is actually associated with the morphological instability of nanometer scale roughness and consequently a signature of the EM mechanism.

Acknowledgment. Funding for this work was provided by the ARO (Grant DAAG55-97-1-0133), NSF (Grant CHE-940078), and the MRSEC program of the NSF (Grants DMR-9632472 and DMR-0076097). The authors are grateful to Dr. John C. Hulteen for the acquisition of AFM data. C.L. Haynes gratefully acknowledges the support of GlaxoSmithKline and the ACS Division of Analytical Chemistry.

References and Notes

(1) Campion, A.; Kambhampati, P. *Chem. Soc. Rev.* **1998**, *27*, 241−250.

(2) Otto, A.; Mrozek, I.; Grabhorn, H.; Akemann, W. *J. Phys. Condens. Matter* **1992**, *4*, 1143−1212.

(3) Cotton, T. M.; Brandt, E. S. Surface-Enhanced Raman Scattering. In *Physical Methods of Chemistry Series: Investigations of Surfaces and Interfaces−Part B*, 2nd ed.; Rossiter, B. W., Baetzold, R. C., Eds.; John Wiley & Sons: New York, 1993; Vol. IXB, pp 633−718.

(4) Moskovits, M. *Rev. Mod. Phys.* **1985**, *57*, 783−826.

(5) Storey, J. M. E.; Barber, T. E.; Shelton, R. D.; Wachter, E. A.; Carron, K. T.; Jiang, Y. *Spectroscopy* **1995**, *10*, 20−25.

(6) Weaver, M. J.; Zou, S. Vibrational Spectroscopy of Electrochemical Interfaces: Some Walls and Bridges to Surface Science Understanding. In *Spectroscopy for Surface Science*; Clark, R. J. H., FRS, Hester, R. E., Eds.; John Wiley & Sons: New York, 1998; Vol. 26; pp 219−272.

(7) Kneipp, K.; Kneipp, H.; Itzkan, I.; Dasari, R. R.; Feld, M. S. *Curr. Sci.* **1999**, *77*, 915−924.

(8) Manfait, M.; Nabiev, I. Applications in Medicine. In *Raman Microscopy. Developments and Applications*; Turrell, G., Corset, J., Eds.; Academic Press/Harcourt Brace & Company: New York, 1996; pp 379−420.

(9) Fabian, H.; Anzenbacher, P. *Vib. Spectrosc.* **1993**, *4*, 125−148.

(10) Douketis, C.; Haslett, T. L.; Wang, Z.; Moskovits, M.; Iannotta, S. *Prog. Surf. Sci.* **1995**, *50*, 187−195.

(11) Van Duyne, R. P.; Hulteen, J. C.; Treichel, D. A. *J. Chem. Phys.* **1993**, *99*, 2101−2115.

(12) Van Duyne, R. P.; Haller, K. L.; Altkorn, R. I. *Chem. Phys. Lett.* **1986**, *126*, 190−196.

(13) Litorja, M.; Haynes, C. L.; Haes, A. J.; Jensen, T. R.; Van Duyne, R. P. *J. Phys. Chem. B* **2001**, *105*, 6907−6915.

(14) Sun, L. Time-Resolved Surface Enhanced Raman Scattering Studies of Substrate Morphology Transformation and Surface Adsorption/Desorption Kinetics at Colloidal and Electrochemical Interfaces. Dissertation, Northwestern University, Evanston, IL, 1990.

(15) Bokor, J. *Science* **1989**, *246*, 1130−1134.

(16) Hofer, U.; Shumay, I. L.; Reuá, C.; Thomann, U.; Wallauer, W.; Fauster, T. *Science* **1997**, *277*, 1480−1482.

(17) Schatz, G. C.; Van Duyne, R. P. Electromagnetic Mechanism of Surface-Enhanced Spectroscopy. In *Handbook of Vibrational Spectroscopy*; Griffiths, P. R., Ed.; Wiley: New York, 2001; pp 1−16.

(18) Schatz, G. C. Electromagnetic Mechanism of Surface Enhanced Spectroscopy. In *Fundamentals and Applications of Surface Raman Spectroscopy*; Garrell, R. L., Pemberton, J. E., Cotton, T. M., Eds.; VCH Publishers: Deerfield Beach, Florida, 1997.

(19) Wasileski, S. A.; Zou, S.; Weaver, M. J. *Appl. Spectrosc.* **2000**, *54*, 761−772.

(20) Haynes, C. L.; Van Duyne, R. P. *J. Phys. Chem. B* **2001**, *105*, 5599−5611.

(21) Otto, A.; Billmann, J.; Eickmans, J.; Ertuerk; Pettenkofer, C. *Surf. Sci.* **1984**, *138*, 319−338.
(22) Choi, Y.-S.; Kim, J.-J.; Miyajima, S. *Chem. Phys. Lett.* **1996**, *255*, 45−48.
(23) Kambhampati, P.; Child, C. M.; Foster, M. C.; Campion, A. *J. Chem. Phys.* **1998**, *108*, 5013−5026.
(24) Campion, A.; Ivanecky, J. E. I. I. I.; Child, C. M.; Foster, M. *J. Am. Chem. Soc.* **1995**, *117*, 11807−11808.
(25) Michaels, A. M.; Nirmal, M.; Brus, L. E. *J. Am. Chem. Soc.* **1999**, *121*, 9932−9939.
(26) Emory, S. R.; Haskins, W. E.; Nie, S. *J. Am. Chem. Soc.* **1998**, *120*, 8009−8010.
(27) Michaels, A. M.; Jiang, J.; Brus, L. *J. Phys. Chem. B* **2000**, *104* (ASAP article, web release date: November 23, 2000.)
(28) Vlčková, B.; Gu, X. J.; Moskovits, M. *J. Phys. Chem. B* **1997**, *101*, 1588−1593.
(29) Haynes, C. L.; Haes, A. J.; Van Duyne, R. P. *Mater. Res. Soc. Symp. Proc.* **2001**, *635*, C.6/1−C.6/6.
(30) Zeman, E. J.; Schatz, G. C. *J. Phys. Chem.* **1987**, *91*, 634−643.
(31) Dick, L. A.; Van Duyne, R. P. *J. Phys. Chem. B* **2001**. In preparation.
(32) Kennedy, B. J.; Spaeth, S.; Dickey, M.; Carron, K. T. *J. Phys. Chem. B* **1999**, *103*, 3640−3646.
(33) Tsen, M.; Sun, L. *Anal. Chim. Acta* **1995**, *307*, 333−340.
(34) Pipino, A. C. R.; Schatz, G. C.; Van Duyne, R. P. *Phys. Rev. B* **1996**, *53*, 4162−4169.
(35) Boyd, G. T.; Rasing, T.; Leite, J. R. R.; Shen, Y. R. *Phys. Rev. B* **1984**, *30*, 519−526.
(36) Chen, T. T.; Von Raben, K. U.; Murphy, D. V.; Chang, R. K.; Laube, B. L. *Surf. Sci.* **1984**, *143*, 369−390.
(37) Li, W.-H.; Li, X.-Y.; Yu, N.-T. *Chem. Phys. Lett.* **1999**, *305*, 303−310.
(38) Yang, W. H.; Hulteen, J. C.; Schatz, G. C.; Van Duyne, R. P. *J. Chem. Phys.* **1996**, *104*, 4313−4323.
(39) Chen, J.-S.; Devine, T. M.; Ogletree, D. F.; Salmeron, M. *Surf. Sci.* **1991**, *258*, 346−358.
(40) Kannen, G.; Otto, A. *Chem. Phys.* **1990**, *141*, 51−61.
(41) Furtak, T. E.; Macomber, S. H. *Chem. Phys. Lett.* **1983**, *95*, 328−332.
(42) Mrozek, I.; Otto, A. On the "First Layer Effect" of SERS from Silver Island Films. In *Recent Trends in Raman Spectroscopy*; Banerjee, S. B., Jha, S. S., Eds.; World Scientific: Singapore, 1989; pp 224−240.
(43) Pettenkofer, C.; Otto, A. *J. Phys. (Paris)* **1983**, *C10*, 1159.
(44) Moskovits, M.; DiLella, D. P. Vibrational Spectroscopy of Molecules Adsorbed on Vapor-Deposited Metals. In *Surface Enhanced Raman Scattering*; Chang, R. K., Furtak, T. E., Eds.; Plenum Press: New York, 1982; pp 243−274.
(45) Ertuerk, U.; Pettenkofer, C.; Otto, A. *J. Electron. Spectrosc. Relat. Phenom.* **1986**, *38*, 113−122.
(46) Gao, Y.; Lopez-Rios, T. *Phys. Rev. Lett.* **1984**, *53*, 2583−2586.
(47) Watanabe, T.; Yanagihara, N.; Honda, K.; Pettinger, B.; Moerl, L. *Chem. Phys. Lett.* **1983**, *96*, 649−655.
(48) Pettinger, B.; Moerl, L. *J. Electron. Spectrosc. Relat. Phenom.* **1983**, *29*, 383−395.
(49) Guy, A. L.; Pemberton, J. E. *Langmuir* **1987**, *3*, 125−132.
(50) Guy, A. L.; Pemberton, J. E. *Langmuir* **1985**, *1*, 518−525.
(51) Pettinger, B.; Moerl, L. *J. Electroanal. Chem.* **1983**, *150*, 415−424.
(52) Macomber, S. H.; Furtak, T. E. *Solid State Commun.* **1983**, *45*, 267−271.
(53) Freunscht, P.; Van Duyne, R. P.; Schneider, S. *Chem. Phys. Lett.* **1997**, *281*, 372−378.
(54) Viets, C.; Hill, W. *J. Raman Spectrosc.* **2000**, *31*, 625−631.
(55) Dick, L. A.; Haes, A. J.; Van Duyne, R. P. *J. Phys. Chem. B* **2000**, *104*, 11752−11762.
(56) Deckert, V.; Zeisel, D.; Zenobi, R.; Vo-Dinh, T. *Anal. Chem.* **1998**, *70*, 2646−2650.
(57) Schueler, P. A.; Ives, J. T.; DeLaCroix, F.; Lacy, W. B.; Becker, P. A.; Li, J.; Caldwell, K. D.; Drake, B.; Harris, J. M. *Anal. Chem.* **1993**, *65*, 3177−3186.
(58) Hulteen, J. C. I. Surface-Enhanced Hyper-Raman Spectroscopy. II. Nanosphere Lithography. Ph.D. Thesis, Northwestern University, Evanston, IL, 1995.
(59) Otsuka, I.; Iwasaki, T. *J. Vac. Sci. Technol. A* **1990**, *8*, 530−533.
(60) Cross, N.; Pemberton, J. E. *J. Electroanal. Chem.* **1987**, *217*, 93−100.
(61) Pemberton, J. E. Surface Enhanced Raman Scattering. In *Electrochemical Interfaces: Modern Techniques for In Situ Interface Characterization*; Abruna, H. D., Ed.; VCH Verlag Chemie: Berlin, 1991; pp 193−263.
(62) Leung, L. W. H.; Weaver, M. J. *Langmuir* **1988**, *4*, 1076−1083.
(63) Wilke, T.; Gao, X.; Takoudis, C. G.; Weaver, M. J. *Langmuir* **1991**, *7*, 714−721.
(64) Lakovits, J. M. Part 1: Resonance Raman Spectroelectrochemistry of the Tetracyanoquinodimethane Dianion. Part 2: Double Potential Step Chronocoulometry Studies of Adsorption on a Silver Electrode. Dissertation, Northwestern University, Evanston, IL, 1981.
(65) Miller, B. E. Surface Enhanced Raman Scattering On Composition Modulated Alloys and Surface and Solution Raman Scattering in the Visible and Ultraviolet. Dissertation, Northwestern University, Evanston, IL, 1989.
(66) Gosser, D. K.; Zhang, F. *Talanta* **1991**, *38*, 715−722.
(67) Kovach, P. M.; Caudill, W. L.; Peters, D. G.; Wightman, R. M. *J. Electroanal. Chem.* **1985**, *185*, 285−295.
(68) Gennett, T.; Weaver, M. J. *Anal. Chem.* **1984**, *56*, 1444−1448.
(69) Fornari, B.; Mattei, G.; Pagannone, M. *J. Vac. Sci. Technol. A* **1988**, *6*, 167−168.
(70) Carron, K. T. Surface Enhanced Resonance Raman, Resonance Hyper-Raman, and Hyper-Raman Spectroscopy of Molecules Adsorbed to Thin Metal Films. Dissertation, Northwestern University, Evanston, IL, 1985.
(71) Bilewicz, R.; Majda, M. *J. Am. Chem. Soc.* **1991**, *113*, 5464−5466.
(72) Tadayyoni, M. A.; Farquharson, S.; Weaver, M. J. *J. Chem. Phys.* **1984**, *80*, 1363−1365.
(73) Beer, K. D.; Tanner, W.; Garrell, R. L. *J. Electroanal. Chem.* **1989**, *258*, 313−325.
(74) Billman, J.; Otto, A. *Surf. Sci.* **1984**, *138*, 1−25.
(75) Jeanmaire, D. L. Resonance Raman and Surface Raman Spectroelectrochemistry. Dissertation, Northwestern University, Evanston, IL, 1977.